Three-dimensional Multi-site Random Access Photostimulation (3D-MAP)

Yi Xue
University of California Berkeley https://orcid.org/0000-0003-2622-083X
Laura Waller
University of California Berkeley https://orcid.org/0000-0003-1243-2356
Hillel Adesnik (hadesnik@berkeley.edu)
Berkeley
Nicolas Pégard
University of North Carolina at Chapel Hill

Article

Keywords: 3D-MAP, optogenetic, 3D multi-site illumination

Posted Date: September 28th, 2020

DOI: https://doi.org/10.21203/rs.3.rs-71257/v1

Version of Record: A version of this preprint was published at eLife on February 10th, 2022. See the published version at https://doi.org/10.7554/eLife.73266.

Abstract

Optical control of neural ensemble activity has been crucial for understanding brain function and disease, yet no technology can achieve optogenetic control of very large numbers of neurons at extremely fast rates over a large volume. State-of-the-art multiphoton holographic optogenetics requires high power illumination that only address relatively small populations of neurons in parallel. Conversely, one-photon holographic techniques can stimulate more neurons but with a trade-off between resolution and addressable volume. We introduce a new one-photon light sculpting technique, termed Three-Dimensional Multi-site random Access Photostimulation (3D-MAP), that simultaneously overcomes all these limitations by dynamically modulating light in both the spatial and angular domain at multi-kHz rates. Electrophysiological measurements confirm that 3D-MAP achieves high spatial precision in vitro and in vivo. Using 3D-MAP, we then interrogate neural circuits with 3D multi-site illumination with high resolution over a large volume of intact brain that existing techniques cannot achieve.

Introduction

Optogenetics enables rapid and reversible control of neural activity[1,2]. By patterning the illumination light[3] with either one-photon[4-12] or two-photon photostimulation[13-18], one can activate or suppress specific neural ensembles in order to map neural circuits, investigate neural dynamics, or attempt to draw links between specific patterns of neural activity and behavior. Two-photon photostimulation has the advantage of high spatial resolution for precise neural activity control and relative immunity to light scattering from tissue, enabling control over deep brain circuits. However, two-photon holographic optogenetics can only stimulate relatively small ensembles of neurons at a time, limited by the very high-power pulsed illumination required for non-linear excitation. Such high energy can heat brain tissue, disturbing brain activity and causing thermal damage[18-19]. The accessible volume for holographic two-photon photostimulation is also limited by the coherence length of the femtosecond pulse laser being used since holographic Multiphoton optogenetic systems are also extremely expensive and sophisticated, and therefore difficult to adopt by the broader neuroscience community.

One-photon photostimulation systems, in contrast, use two to three orders-of-magnitude less laser power, which are much simpler to implement and far less expensive. Under conditions of limited light scattering, such as superficial brain structures, *ex vivo* experiments, or relative transparent organisms, they can achieve high resolution photostimulation. There are three main strategies to generate multiple foci with one-photon photostimulation, yet none is capable of simultaneously stimulating specific multiple neural ensembles over a large 3D volume with high spatial resolution. The first approach, scanning-based one-photon photostimulation, stimulates neurons sequentially by rapidly scanning a single focus across small neural clusters with scanning mirrors[22] or acousto-optic deflectors (AODs)[23-24]. This method cannot photo-stimulate distributed ensembles simultaneously. The second approach is to directly project 2D illumination patterns onto samples with a Digital Micromirror Device (DMD)[8-12]. This widefield illumination scheme has a large field-of-view (FOV) and moderate lateral resolution but only modulates

light in 2D. The axial resolution is poor and yields unwanted photostimulation above and below the focal plane. The third approach, Computer Generated Holography (CGH), generates 3D distributed foci by phase modulation in Fourier space using a spatial light modulator (SLM)[4-7]. One-photon CGH has high lateral resolution and moderate axial resolution, but has several critical drawbacks that constrain its ability to execute sophisticated optogenetics experiments. First, its FOV is relatively small at high spatial resolution. The throughput of CGH is limited by the number of degrees of freedom (DoF) that is determined by the number of pixels and bit depth of the SLM, regardless of magnification and numerical aperture. Second, the refresh rate of the SLMs and the hologram computation limit the speed of CGH. The refresh rate of SLMs is more than an order-of-magnitude slower compared to that of standard DMDs and computing a 2D phase mask at the Fourier plane for a 3D hologram pattern is an ill-posed problem that requires iterative optimization[25-28]. The extra computational requirements for generating hologram patterns (rather than directly projecting patterns on a DMD) can become limiting when thousands of different patterns are required (as in high throughput mapping experiments), or when fast online computation of these patterns is needed for closed-loop experiments. The third drawback of one-photon CGH is that holograms composed of increasing spot number will increase spatial cross-talk as out-of-focus light from each focus interact, accidentally stimulating neurons that are not meant to be targeted. Taken together, despite the power of these one photon techniques, none are suitable for large-scale high resolution optogenetic activation of distributed ensembles of neurons.

To overcome this challenge, we developed 3D multi-site random access photostimulation (3D-MAP), a new approach to generate 3D illumination patterns by modulating light both in the angular domain, , with scanning mirrors and in the spatial domain, , with a DMD. For 3D optogenetic photostimulation, illumination patterns must be optimized to target a photosensitive opsin expressed neuronal soma (~10μm). The set of light rays needed to generate each spherical target can be described as a hyperplane within the 4D light field spatio-angular domain, , and these rays can be generated by rapidly sweeping through the appropriate angles of illumination (with the scanning mirrors) while projecting the corresponding amplitude masks of spatial apertures (with the DMD). 3D-MAP allows one DMD frame for each unique orientation of the scanning mirrors, hence the total number of DoF is much larger than existing one-photon optogenetic stimulation techniques[4-12]. Compared to 2D widefield patterning methods, 3D-MAP retains the advantages of high-throughput and computational efficiency, while extending the addressable space from 2D to 3D. Compared to CGH, 3D-MAP dramatically increases the number of DoF that achieves both high spatial resolution and large accessible volume, as well as generates illumination patterns that CGH cannot synthesize. Therefore, 3D-MAP is able to reduce spatial cross-talk by sculpting the 3D optical stimulation pattern so as to minimize the stimulation of non-targeted areas. 3D-MAP also patterns the entire addressable volume at multi-kHz rate (the volumetric pattern refresh rate), which exceeds the bandwidth of most neural circuits and is one order of magnitude faster than 3D CGH. Due to the advantage of high-speed, 3D-MAP can project several different patterns within a stimulation period, which not only increases the total number of foci but also further reduces cross-talk especially when the density of targets is high. CGH cannot mitigate spatial cross-talk with these strategies and therefore the number and accessible location of the foci remain limited. For

reference, a comparison between strengths and weaknesses of 3D-MAP versus existing photostimulation approaches is shown in Supplementary Table 1, and a comparison of 3D spatial resolution is shown in Supplementary Figure 1. In summary, 3D-MAP is the first light sculpting method to achieve high spatial resolution, large FOV and high modulation speed at the same time.

We present the experimental setup and computational methods to synthesize custom 3D illumination patterns, and we empirically demonstrate that 3D-MAP achieves high resolution photostimulation in brain slices and *in vivo* recorded by electrophysiology. We then use 3D-MAP to perform high-throughput synaptic connectivity mapping *in vitro* and *in vivo*, using both single-spot illumination and multi-spot illumination in 3D. These experiments validate 3D-MAP as a one-photon technique to manipulate neural circuits on-demand with high spatiotemporal resolution in the intact brain. It can be flexibly used to map neural connectivity at both small and large scales and correlate causally related complex activity patterns to behavior.

Results

Optical Design of 3D-MAP

The experimental setup for 3D-MAP is shown in Figure 1. A DMD modulates amplitude in real space, (x,y), while scanning mirrors control the angles of illumination, (k_x,k_y) . Both devices are placed at conjugate image planes (Fig. 1a) and time-synchronized. We first compute the light field parameters (x, y, k_x, k_y) of each beam, and display these amplitude masks of spatial apertures with the matching illumination angles one-by-one (Fig. 1b). These amplitude masks can be located at any place at the native focal plane (Fig. 1c). For the simplest case (Fig. 1b), the aperture on the DMD rotates in a circle as we sweep through each projection angle set by the scanning mirrors. The center of the circle matches the lateral position of the target, and the diameter of the aperture displacement circle, D, determines its axial position. These amplitude masks are computed by ray tracing the perspective views of the target back to the objective's native focal plane. A larger diameter of the aperture displacement circle corresponds to a target placed further away from the image plane. Clockwise and counterclockwise rotations of the projection correspond to a target located above or below the native focal plane. When the target is at the native focal plane (z=0), the diameter D is zero and we simply turn on the pixels corresponding to the desired position. Conventional CGH systems synthesize a 3D hologram pattern by modulating a coherent laser beam with a 2D static phase mask at the conjugate Fourier plane, which is an ill-posed problem where the 3D pattern is an approximate solution. These foci in the hologram pattern are subject to speckle, and the out-of-focus light along the z-axis generates cross-talk in the non-targeted areas right above and below the targeted area. Conversely, 3D-MAP modulates light incoherently in time to eliminate speckle, and reduces the cross-talk by not selecting certain illumination angles to avoid stimulating non-targeted areas, further enhancing the stimulation accuracy and efficiency (Fig. 1c). To simultaneously activate multiple neurons, we generate a multi-site photostimulation pattern by superimposing the light field parameters corresponding to each target (Fig. 1d).

The axial resolution of 3D-MAP can be improved by increasing the number of beams that are sequentially projected to generate the focus (Fig. 1e-f). However, more amplitude masks require more on-chip memory space of the DMD. Increasing the number of masks will reduce the projection time of each mask but the total simulation time is the same, because the minimum projection time of the DMD (77μs) is about 52-fold shorter than the stimulation time (4ms, see later sections for details). In all experiments, we decided to overlap the beam from 10 high illumination angles to generate high resolution patterns, since the improvement of axial resolution is moderate with additional illumination angles (Fig. 1f). The refresh rate of the DMD is 13kHz, and each 3D volumetric pattern is generated by 10 masks on the DMD, so the volumetric pattern rate is 1.3kHz, which is much faster than commercial SLMs (low hundreds of Hertz). Since the characteristic timescale of the microbial opsin is much longer than the duration of individual projection masks, the relevant light sculpting pattern is the time-averaged sum of the intensity of several mutually incoherent masks. In addition, the computing speed of masks in 3D-MAP is based on ray tracing and can be calculated much faster than in CGH[25-28]. 3D-MAP is a new method to sculpt light in 3D and enables new real-time applications such as mapping neural circuits (see Figure 1).

Optical Characterization of 3D-MAP

3D-MAP can stimulate multiple targets across a large FOV at very high spatiotemporal resolution. To quantify the spatial resolution of 3D-MAP, we turned on one pixel of the DMD (acting as a point source) and measured the 3D optical point-spread-function (PSF) by imaging a thin fluorescent film on a microscope slide at many depth planes (Fig. 2a-c). The full-width-half-maximums (FWHMs) of the resulting 3D PSF indicate a spatial resolution of 5x5x18μm^3. We also demonstrated the ability to simultaneously generate 25 foci at custom (x, y, z) locations in a 744x744x400 μm^3 volume (Fig. 2d), with more examples of multi-spot generation in Supplementary Figure 2. Thus, 3D-MAP achieves high spatial resolution for multi-site stimulation over a large volume.

We next evaluated the influence of tissue scattering on focusing capabilities with 3D-MAP by measuring the size of a target after propagating through acute brain slices (brain slices that are kept vital *in vitro* for hours) of increasing thickness on top of the thin fluorescent film (Fig. 2e). We generated a focused target by turning on a 10-pixel radius aperture on the DMD (8μm in diameter at the native focal plane) to produce an illumination volume matching the typical dimensions of a neuronal soma in the cortex. Notice that this target size is not illustrative of the spatial resolution limit of 3D-MAP, but represents a practical choice of 3D pattern that matches the size of neurons and our application. We compared scattering for both blue (473nm) and red (635nm) excitation light. Without the brain slice, the size of the focus was 11.7x11.7x42μm^3 (blue) and 10.4x10.4x50.7μm^3 (red). When generating the focus through 50μm, 100μm and 150μm thick brain slices, the size of the focus spot with blue light increased by 8%, 75%, and 269%, and the size of the focus spot with red light increased by 67%, 107%, and 114%, respectively. Even though the spatial resolution degrades as the brain slice becomes thicker, the effective optical resolution of 3D-MAP is on the order of a single or very small cluster of neurons. In brain tissue, Rayleigh scattering affects red light much less than blue light, so photostimulation with red light maintains high resolution in

brain areas that are deeper than 100μm. Thus, 3D-MAP should be able to stimulate neurons in brain slices or superficial layers *in vivo* at high spatial resolution.

3D-MAP Photostimulation with very high spatial resolution in brain tissue

We next quantified the physiological spatial resolution as measured by the physiological point spread function (PPSF) of 3D-MAP by stimulating neurons in acute mouse brain slices and *in vivo*. We made whole cell patch clamp recordings from L2/3 excitatory neurons expressing the potent, soma-targeted optogenetic protein ChroME[18] (see Methods). The PPSF records the photocurrent response as a function of the displacement between the targeted focus and the patched cell[17]. Because ChroME has a non-linear response to light intensity[18], it is necessary to measure PPSF in addition to optical PSF to quantify the physiological spatial resolution. Since 3D-MAP is able to calculate and project patterns much faster than CGH[25-28], we measured the volumetric PPSF by recording the photocurrent response from 2,541 targeted locations (a 11x11x21 pixels grid) in 2-5 minutes, limited only by opsin kinetics (4ms photostimulation followed by 8-40ms relaxation time at each pixel, varying by opsin). The PPSF measurements show that 3D-MAP provides near single-cell resolution photostimulation *in vitro* (lateral FWHM, 29±0.8μm; axial FWHM, 44±1.6μm, 9 cells, Fig. 3a-c), only approximately two-fold worse than prior measurements with multiphoton optogenetics[17-18, 29.] We also measured the spiking probability of neurons in acute brain slices and in living mice along the lateral and axial dimensions in order to quantify the physiological resolution of 3D-MAP for supra-threshold neuronal activation. While patching the neuron, we digitally displaced the target generated by 3D-MAP along the x-axis and z-axis. The result also demonstrates very high spatial resolution under these conditions (Fig. 3d-e, *in vitro* results, lateral FWHM, 16±2.4μm; axial FWHM, 44±8.9μm, 5 cells; Fig. 3i-j, *in vivo* results, lateral FWHM, 19±3.7μm; axial FWHM, 45±6.1μm, 8 cells). Together, these data validate 3D-MAP as a novel scanless 3D one-photon light sculpting technique for optogenetic stimulation with very high spatiotemporal resolution in the mouse brain.

High throughput synaptic connectivity mapping over large volumes with 3D-MAP

In addition to high spatiotemporal resolution and fast computational speed, 3D-MAP is easily scalable and can address large volumes at various stimulation powers. To demonstrate these advantages, we used 3D-MAP to probe synaptic connectivity in 3D (Fig. 4). We expressed ChroME in excitatory neurons of the cortex (see Methods), then made whole cell voltage clamp recordings from inhibitory interneurons that do not express ChroME under these conditions, to avoid the confounding effect of direct photocurrents in the patched neuron (Fig. 4a). The wide-field fluorescent image (Fig. 4b) shows the excitatory neurons (red) and the patched inhibitory interneuron (green). We first mapped an 800x800μm^2 FOV at low spatial sampling (40μm grid) to identify a sub-region that contained most of the presynaptic neurons (Fig. 4c), and then mapped that sub-region at fine resolution (20μm/pixel, Fig. 4d) and even higher resolution (9μm/pixel, Fig. 4e). Due to variable opsin protein expression levels across neurons, as well as variable intrinsic neural excitability, neurons are differentially sensitive to light. By mapping the same sub-region at different power levels, we could take advantage of this fact to help identify putative individual (i.e., ‘unitary’) sources of presynaptic input (Fig. 4d). Photostimulation generated excitatory

postsynaptic currents (EPSCs) at many locations, and importantly, most connectivity maps exhibited spatial clusters like synaptic input maps in space (Fig. 4d-e). Within each cluster, most of the postsynaptic responses had similar amplitudes and time courses, suggesting they primarily arose from just one or a small number of presynaptic neurons (Fig. 4f-g). We also performed the synaptic connectivity mapping *in vivo* (Fig. S3). These results demonstrate that 3D-MAP is easily scalable and suitable for obtaining high resolution connectivity maps of neural circuits.

One of the major advantages of 3D-MAP over conventional single point scanning approaches[22-24] is that it has the capacity to stimulate multiple neurons distributed anywhere in the addressable volume simultaneously. Multi-site photostimulation is crucial for perturbing or mapping brain circuits because only the activation of neural populations can drive the sophisticated activity patterns needed to understand network dynamics or behavior[30]. Thus, we next demonstrated that 3D-MAP is able to simultaneously stimulate multiple user-defined targets (Fig. 5). While patching the same inhibitory interneuron as described above (Fig. 5b, the same as Fig. 4e), we first stimulated the 5 presynaptic ROIs revealed in the widefield mapping experiment above one-by-one, and then stimulated subsets of them simultaneously, and finally stimulated all the ROIs together (Fig. 5c). We compared the photocurrents measured by multi-site simultaneous stimulation (Fig. 5d, blue, stimulation of all the ROIs) to the linear sum of individual responses by single stimulation (Fig. 5d, red, the sum of the first row of Fig. 5c) and observed the multi-site stimulation generates greater net input (Fig. 5e, $p=0.0488$ for 2-5 sites stimulation, two-way analysis of variance (ANOVA)). This example shows that 3D-MAP is able to simultaneously stimulate multiple targets and also can flexibly adjust the 3D patterns in real time, which is important for online interrogation of neural circuits.

Reconstructing synaptic networks with 3D-MAP via gradient descent

Physiological brain mapping approaches must overcome the challenge of temporal throughput to map ever larger regions of brain tissue. We reasoned that mapping neural circuits with multiple foci, rather than a single focus, could scale up the temporal throughput of the system dramatically, since the overall connectivity matrix is remarkably sparse. Instead of randomly shifting a single focus to measure the one-to-one synaptic connections (Fig. 4), we used 3D-MAP to stimulate multiple random voxels simultaneously and reconstructed the spatial map of presynaptic networks via gradient descent. Notice that the positions of the simultaneously stimulated voxels were randomly distributed in the 3D volume and the neural connections are unknown, unlike co-stimulating known presynaptic ROIs in the last section (Fig. 5). In acute brain slices we again patched a GABAergic interneuron under voltage-clamp mode and recorded both EPSCs, and subsequently, inhibitory postsynaptic currents (IPSCs). We projected random sets of foci (five at a time) and repeated this process until all voxels in 3D were stimulated several times (typically 5-10). Treating the recorded photocurrents as a combination of responses from multiple sites, we used an optimization algorithm based on gradient descent to reconstruct the map of the synaptic network (see Methods).

Results in Fig. 6 show the excitatory synaptic network map and inhibitory synaptic network map of the same GABAergic interneuron in an 800x800x200μm^3 volume at three different stimulation powers. Multi-site simultaneous stimulation has two key advantages. First, perhaps more importantly, multi-site stimulation engages the activity of spatially distributed ensembles of neurons (rather than single neurons or small local clusters), which may facilitate polysynaptic network activity and engage network level properties of the circuit. Second, it is possible to reconstruct the same mapping results with fewer measurements compared to single-target stimulation based on compressive sensing, assuming the multiple stimulation sites are sparse and the readout signal is a linear combination of the inputs from these sites. The assumption is valid when the multiple voxels for concurrent stimulation are randomly drawn from the volume and the number of these voxels is much smaller than the total voxels in the volume (5 voxels are randomly drawn from 1600 voxels in our experiment). Since multiple voxels are stimulated at the same time (say N voxels), each voxel needs to be measured N times with different patterns to distinguish the current from each voxel. Under the assumption of sparsity and linearity, we can reconstruct the map of neural networks using compressive sensing with less repetitions (Fig. S4, Methods). This feature of 3D-MAP is important to speed up the mapping of a large volume where single-target stimulation of every voxel would take too long.

Discussion

In this study we demonstrated and validated 3D-MAP, a one-photon technique that enables 3D multi-site random access illumination for high precision optogenetic photostimulation. 3D-MAP combines novel computational and optical advances to offer an extremely powerful and flexible optical brain perturbation system. Unlike prior one-photon approaches that have low spatial resolution (DMD-based 2D projection)[8-12] or small FOV (SLM-based 3D CGH)[4-7], 3D-MAP achieves high spatial precision at extremely high speeds and in large 3D volumes in the superficial layers of the intact brain. 3D-MAP is the first system to achieve 3D multi-site illumination with previously unattainable DoF by simultaneously sculpting the light field in both intensity and angular domains. Therefore, 3D-MAP is able to generate high resolution 3D patterns over large volumes that CGH cannot synthesize. 3D-MAP is also able to project 3D patterns at much faster speeds than CGH not only because the refresh rate of the DMD is an order of magnitude faster than that of an SLM, but also because calculating the light field parameters with ray tracing in 3D-MAP is much faster than calculating phase masks in 3D CGH.

Both one-photon and two-photon multi-site photostimulation are subject to spatial cross-talk, as out-of-focus light from one target may accidentally stimulate neurons that are at other focal planes, especially when the density of foci is high or when out-of-focus neurons are more photosensitive than the desired targets. 3D-MAP's large DoF and high speed should allow users to stimulate densely labeled neurons with less spatial cross-talk than CGH. It achieves this with two strategies: first, 3D-MAP is able to generate light patterns that specifically illuminate targeted areas but minimize illumination of non-targeted areas at other focal planes by generating an 'empty cone' for each target of illumination, effectively dumping out-of-focus light diffusely elsewhere (Fig. 1c, Fig. S1). Such light patterns cannot be synthesized with CGH.

Second, when the desired density of foci is high and cross-talk could be severe, 3D-MAP can leverage its higher volumetric rate to exploit the temporal domain by multiplexing patterns that target smaller subsets of neurons at a time in order to increase pattern sparsity, thus mitigating spatial cross-talk.

Like any other one-photon photostimulation technique, the effective resolution of 3D-MAP in brain tissue is determined by scattering. As we show in Figure 2, illumination with red light can reduce Rayleigh scattering and mitigate resolution loss through brain tissue, but stimulation depth is still limited to the first few hundreds microns below the surface of the mouse brain. To photo-stimulate neurons deeper inside the mammalian brain with 3D-MAP, the cortex can be removed or implemented with a miniaturized microscope as it is routinely performed to image deep structures such as the hippocampus or the thalamus[5, 31-33]. Taken together, 3D-MAP is a new volumetric optogenetic projection system that offers major advantages over existing one-photon and two-photon optogenetic technologies and should facilitate a wide range of neural perturbation experiments to map the structure and function of brain circuits.

Methods

Ethical statement. All animal experiments were performed in accordance with the guidelines and regulations of the Animal Care and Use Committee of the University of California, Berkeley.

Data availability. The datasets generated during and/or analyzed during the current study are available upon reasonable request to the corresponding authors.

Code availability. Custom code used to collect and analyze data is programed in MATLAB. The code has been deposited in Github (https://github.com/Waller-Lab/3D-MAP).

3D-MAP optical setup. The laser sources for optogenetic stimulation are Diode Pumped Solid State (DPSS) laser diodes. One is at 473nm wavelength (MBL-N-473A-1W, Ultralasers, Inc., Canada) and the other at 635nm wavelength (SDL-635-LM-5000T, Shanghai Dream Lasers Technology Co., Ltd., China) for different opsins. The results shown in Fig. 6 are measured under red stimulation, and all the others are stimulated by blue light. The laser source for *in vivo* PPSF (Fig. 3f-g) and wide-field imaging (Fig. 4b) is a DPSS laser at 589nm wavelength (MGL-W-589-1W, Ultralasers, Inc., Canada). Current supplies are externally driven by an analog modulation voltage. The laser beams are scanned by a pair of galvo-mirrors (GVS202, Thorlabs, Inc., U.S.), and then the beam size is expanded to fill the DMD (DLP9000X and the controller V4390, ViALUX, Germany) by a 4-f system (f_1=45mm, f_2=150mm). The DMD is mounted on a rotation base in order to maximize the output laser power from 'ON' pixels and minimize the diffraction pattern from DMD pitches. Then the patterned beam passes through a tube lens (f=180mm) and the objective lens (XLUMPlanFL N, 20x, NA 1.0, Olympus) to generate multiple foci. The objective lens is mounted on a motorized z-stage (FG-BOBZ-M, Sutter Instrument, U.S.). A custom dichroic mirror (zt473/589/635rpc-UF2, Chroma, U.S.) is placed before the objective lens to reflect the stimulation laser beams while transmitting fluorescence photons emitted from the sample. The wide-field fluorescence

image (Fig. 4b) is recorded by a camera (Prime95B, Teledyne Photometrix, U.S.). Brain samples (acute brain slices and anesthetized mice) are placed on a motorized x-y stage (X040528 and the controller MP-285, Sutter Instrument, U.S.). The 3D pattern (Fig. 2 and Fig. S2) is measured by capturing the fluorescence excitation in a thin fluorescent film on a microscope slide, with a sub-stage objective (XLUMPlanFL N, 20x, NA 1.0, Olympus) coupled to a camera (DCC1545M, Thorlabs, U.S.). The targeted positions in a 3D pattern are stimulated in a random order: two sequential stimulations are separated by a minimum distance calculated by Poisson disc sampling in order to avoid photocurrent accumulation caused by repeat stimulations. Tomographic renderings of the 3D-MAP illumination patterns are obtained by mechanically scanning the illumination objective along the optical (z) axis and recording the 2D fluorescence image stacks at linearly spaced depths with the sub-stage camera. A NI-DAQ (National Instruments, NI PCIe-6363) synthesizes custom analog signals to synchronously modulate the lasers, the galvo-mirrors, as well as digital triggers to flip frames on the DMD. An analog input channel enabling synchronous measurements of neural photocurrents and spikes in direct response to the custom 3D light sculpting sequence. A custom MATLAB (MathWorks, U.S.) graphic user interface is used to control the NI DAQ boards, calibrate and align the photostimulation and imaging modalities, and for data acquisition and processing.

Computational reconstruction framework.

3D-MAP projects N foci simultaneously in a 3D volume (V voxels), which is defined as a stimulation pattern (th pattern). The positions of the N foci are randomly selected from the V voxels. The electrophysiology readout (excitatory postsynaptic currents, EPSCs; or inhibitory postsynaptic currents, IPSCs) under this pattern is recorded and the maximum absolute value of the EPSCs or IPSCs is the measurement under the illumination of th pattern. Thus, the forward model of multi-site random simultaneous illumination is (Fig. 6a):

$$y_i = \sum_{j=1}^{V} A_{i,j} x_j,\ i = 1, 2, \ldots, P.$$

P is the number of patterns and all patterns are orthogonal to each other. To solve the synaptic connection map at the jth voxel (x_j), the number P should be equal to V. The reconstruction framework can be formulated as l_1- regularized optimization problem that seeks to estimate x by minimizing the difference between the measured currents (y) and those expected via the forward model (Fig. 6b):

$$\underset{x \geq 0}{\operatorname{argmin}}(\|\boldsymbol{Ax} - \boldsymbol{y}\|_2^2 - \lambda R(\boldsymbol{x})),$$

where $R(x)$ describes total-variation (TV) regularization defined as

$$R(\boldsymbol{x}) = \sum_{j=1}^{V} |x_{j+1} - x_j|.$$

This optimization problem is solved using fast iterative shrinkage-thresholding algorithm (FISTA), which is a first-order gradient descent algorithm. FISTA is able to reconstruct the result (Fig. 6c-d, Fig. S4) in real time during the experiments. The algorithm is summarized in Algorithm 1.

Algorithm 1. 3D-MAP algorithm

1. **Procedure** 3D-MAP multi-sites mapping reconstruction
2. Initialize x_0 by uniformly distributed random numbers between [0 1]
3. $k \leftarrow 0$
4. **while** $k < maxiter$ **do**
    a. Gradient $\Delta \boldsymbol{x} \leftarrow FISTA[\boldsymbol{x}_0, \boldsymbol{A}, \boldsymbol{y}, \lambda]$
    b. $\boldsymbol{x}_{k+1} = \boldsymbol{x}_k - \mu \Delta \boldsymbol{x}_k$, where μ is the step size
    c. $k = k + 1$
5. **return** $\boldsymbol{x}$

If every voxel is illuminated M times (the number of repetitions) using P patterns and each pattern illuminates N voxels, we can draw the relation between these parameters:

$$P = MV/N.$$

To solve *x*, P should be equal to V, that is, the number of repetitions (M) should equal to the number of foci (N) in each pattern. However, the number of repetitions could be smaller than M if the multiple illumination foci satisfy these two assumptions: first, the foci are distributed sparsely in the volume; second, the readout postsynaptic current is a linear combination of the response from presynaptic neurons stimulated by these foci. As shown in Fig. S4, where the number of foci is five (N=5), it is possible to reconstruct the synaptic connection map coarsely with less than five repetitions (M=1-4) with compressive sensing algorithms.

Animal preparation and electrophysiology

Neonatal mice age P3-P4 (wild type, emx1-IRES-Cre (JAX stock#005628), or emx1-Cre;GAD67-GFP (MGI:3590301)) were cryoanesthetized on ice and mounted in a head mold. AAVs driving Cre-dependent expression of either soma-targeted ChroME (Fig. 4-5, Fig. S3-4) or Chrimson (Fig. 6) were injected via a Nanoject3 (Drummond) into the visual cortex (~1-2 mm lateral to lambda, 3 sites, 22 nL/ site), ~100-300 microns below the brain surface. In wild type mice we injected AAV-mDlx-ChroME to drive opsin expression in cortical interneurons. All expression vectors co-expressed nuclear targeted mRuby3. Mice were used for brain slice or *in vivo* recordings at P28-P56. Brain slices were prepared as previously described[34]. Slices were transferred to a chamber and perfused with ACSF (no receptor blockers) warmed

to ~33 degrees Celsius. First the microscope objective was centered over the area of V1 with the highest expression density of the opsin, as indicated by the density of mRuby3-expressing cells. ACSF contained in mM: NaCl 119, KCl 2.5, $MgSO_4$ 1.3, $NaH_2PO_4$1.3, glucose 20, $NaHCO_3$ 26, $CaCl_2$ 2.5. Internal solutions contained $CsMeSO_4$ (for voltage clamp) or KGluconate (for current clamp) 135 mM and NaCl 8 mM, HEPES 10 mM, Na_3GTP 0.3 mM, MgATP 4 mM, EGTA 0.3 mM, QX-314-Cl 5 mM (voltage clamp only), TEA-Cl 5mM (voltage clamp only). For loose-patch experiments pipettes were filled with ACSF. The resistance of the patch electrodes ranged from 3-5 megaohms. For direct recording of photocurrents or light induced spiking, we patched neurons (either in loose patch or whole cell patch clamp) that expressed mRuby3. For recording light-driven synaptic inputs we patched from unlabeled putative interneurons (that did not have pyramidal morphology), or from GFP-expressing neurons in GAD67-GFP mice.

For optogenetic mapping we generated light spots ~10 microns wide (apertures of 10-20 pixels in radius on DMD). The total stimulation duration was 3-6 milliseconds. For ChroME-expressing animals we used 473 nm light (Fig. 3a-e, Fig. 4-5, Fig. S3-4), and for Chrimson we used 635 nm light (Fig. 6). All mapping used fully randomized sequences. For measurement of PPSFs and multi-spot synaptic maps we used the system in full 3D mode (Fig. 3, Fig. 5-6, Fig. S4). For single spot synaptic maps all photo-stimuli were at the native focal plane, and the microscope was moved mechanically under software control to obtain input maps at different axial planes (Fig. 4, Fig. S3). Mapping at the native focal plane requires only one DMD mask per light stimulus as compared to ten for a full 3D pattern, allowing for many more masks to be stored in the DMD RAM and rapidly displayed. Galvo-mirrors scan continuously in 2π to enable z-section when mapping at the native focal plane, which is different from direct 2D projection. At the beginning of each mapping experiment we first took a ten-point laser-power dose response curve of the photocurrent or light-induced synaptic current and used this data to choose the power range for photocurrent or synaptic mapping. For spiking PPSFs, the lowest light level that reliably generated spikes when directly targeting the soma was used. For single spot mapping we updated the DMD pattern at 40-80 Hz. For multi-spot mapping we updated the DMD pattern at 10-20 Hz, which minimized network adaptation.

For *in vivo* recording, mice were sedated with chlorprothixene (0.075 mg) and anesthetized with isoflurane (1.5-2%). A small stainless steel plate was attached to the skull with Metabond. The skull was protected with cyanoacrylate glue and dental cement (Orthojet). A 2.5 mm craniotomy was made over V1 with a circular biopsy punch. The dura was removed with fine forceps and the craniotomy was covered with 1.2% agarose in ACSF and additional ACSF. The mouse was then injected with urethane for prolonged anesthesia (0.04 g), and supplemented with 0.5-1.5% isoflurane at the recording rig. Body temperature was maintained at 35-37 degrees Celsius with a warming blanket. Neurons were recorded under visualization either with epifluorescence (to target opsin expressing neurons in the upper 100 microns of the brain for PPSF measurements) or in L2/3 via oblique infrared contrast imaging via an optic fiber (200μm diameter) placed at a ~25 degree angle from horizontal located as close as possible

to the brain surface underneath the objective. The same procedure for optogenetic mapping used *in vitro* was used *in vivo*. All data analysis was performed in MATLAB.

Declarations

Acknowledgements: This work was supported by DARPA N66001-17-C-40154 to H.A. and L.W., as well as NIH UF1NS107574 to H.A. and L.W. This work was supported by the New York Stem Cell Foundation. H.A. is a New York Stem Cell Foundation Robertson Investigator. This work was funded by the Gordon and Betty Moore Foundation's Data-Driven Discovery Initiative through Grant GBMF4562 to L.W. This work was also funded by Burroughs Wellcome Fund, Career Award at the Scientific Interface (5113244) to N.P..

Author contributions

All authors contributed to the development of 3D-MAP. N.P. developed the pilot version of 3D-MAP and the algorithm of 3D image synthesis. Y.X. designed and assembled the current experimental setup, performed simulation and experimental measurements for the optical characterization of the PSF, developed the optimization reconstruction algorithm, and performed data processing in all sections. H.A. designed and performed electrophysiology experiments in mouse brain slice and in anesthetized mouse and advised the research. Y.X. and H.A. wrote the manuscript with additional input form N.P and L.W.. L.W. helped advise Y.X. and N.P.

References

1. Deisseroth, K. Optogenetics. *Methods* **8**, 26–29 (2011).
2. Zhang, F. *et al.* Multimodal fast optical interrogation of neural circuitry. *Nature* **446**, 633–639 (2007).
3. Ronzitti, E. et al. Recent advances in patterned photostimulation for optogenetics. J. Opt. 19, 113001 (2017)
4. Lutz, C. et al. Holographic photolysis of caged neurotransmitters. Nat. Methods 5, 821–827 (2008)
5. Szabo, V., Ventalon, C., De Sars, V., Bradley, J. & Emiliani, V. Spatially selective holographic photoactivation and functional fluorescence imaging in freely behaving mice with a fiberscope. *Neuron* **84**, 1157–1169 (2014).
6. Anselmi, F., Ventalon, C., Bègue, A., Ogden, D. & Emiliani, V. Three-dimensional imaging and photostimulation by remote-focusing and holographic light patterning. *Natl. Acad. Sci. U. S. A.* **108**, 19504–19509 (2011).
7. Reutsky-Gefen, I. et al. Holographic optogenetic stimulation of patterned neuronal activity for vision restoration. Nat. Commun. 4, 1509 (2013)
8. Dhawale, A. K., Hagiwara, A., Bhalla, U. S., Murthy, V. N. & Albeanu, D. F. Non-redundant odor coding by sister mitral cells revealed by light addressable glomeruli in the mouse. Nat. Neurosci. 13, 1404–1412 (2010)

9. Leifer, A. M., Fang-Yen, C., Gershow, M., Alkema, M. J. & Samuel, A. D. T. Optogenetic manipulation of neural activity in freely moving Caenorhabditis elegans. Nat. Methods 8, 147–152 (2011)
10. Adam, Y. *et al.* Voltage imaging and optogenetics reveal behaviour-dependent changes in hippocampal dynamics. *Nature* **569**, 413–417 (2019).
11. Werley, C. A., Chien, M.-P. & Cohen, A. E. Ultrawidefield microscope for high-speed fluorescence imaging and targeted optogenetic stimulation. *Opt. Express* **8**, 5794–5813 (2017)
12. Sakai, S., Ueno, K., Ishizuka, T. & Yawo, H. Parallel and patterned optogenetic manipulation of neurons in the brain slice using a DMD-based projector. *Res.* **75**, 59–64 (2013).
13. Carrillo-Reid, L., Han, S., Yang, W., Akrouh, A. & Yuste, R. Controlling Visually Guided Behavior by Holographic Recalling of Cortical Ensembles. *Cell* **178**, 447–457.e5 (2019).
14. Naka, A. *et al.* Complementary networks of cortical somatostatin interneurons enforce layer specific control. *Elife* **8**, (2019).
15. Nikolenko, V. *et al.* SLM Microscopy: Scanless Two-Photon Imaging and Photostimulation with Spatial Light Modulators. *Neural Circuits* **2**, 5 (2008).
16. Papagiakoumou, E. *et al.* Scanless two-photon excitation of channelrhodopsin-2. *Methods* **7**, 848–854 (2010).
17. Pégard, N. C. *et al.* Three-dimensional scanless holographic optogenetics with temporal focusing (3D-SHOT). *Commun.* **8**, 1228 (2017).
18. Mardinly, A. R. *et al.* Precise multimodal optical control of neural ensemble activity. *Neurosci.* **21**, 881–893 (2018).
19. Podgorski, K. & Ranganathan, G. Brain heating induced by near-infrared lasers during multiphoton microscopy. J. Neurophysiol. 116, 1012–1023 (2016)
20. Sun, S., Zhang, G., Cheng, Z., Gan, W. & Cui, M. Large-scale femtosecond holography for near simultaneous optogenetic neural modulation. *Express* **27**, 32228–32234 (2019).
21. Yang, S. J. et al. Extended field-of-view and increased-signal 3D holographic illumination with time-division multiplexing. Opt. Express 23, 32573–32581 (2015)
22. Petreanu, L., Mao, T., Sternson, S. M. & Svoboda, K. The subcellular organization of neocortical excitatory connections. Nature 457, 1142–1145 (2009)
23. Losavio, B. E., Iyer, V., Patel, S. & Saggau, P. Acousto-optic laser scanning for multi-site photo-stimulation of single neurons in vitro. J. Neural Eng. 7, 045002 (2010)
24. Wang, K. et al. Precise spatiotemporal control of optogenetic activation using an acousto-optic device. PLoS One 6, e28468 (2011)
25. Zhang, J., Pégard, N., Zhong, J., Adesnik, H. & Waller, L. 3D computer-generated holography by non-convex optimization. *Optica, OPTICA* **4**, 1306–1313 (2017).
26. GERCHBERG & W, R. A practical algorithm for the determination of phase from image and diffraction plane pictures. Optik 35, 237–246 (1972)

27. Leseberg, D. Computer-generated three-dimensional image holograms. Appl. Opt. 31, 223–229 (1992)
28. Xue, Y. *et al.* Scanless volumetric imaging by selective access multifocal multiphoton microscopy. *Optica* 6 76 (2019).
29. Prevedel, R. *et al.* Fast volumetric calcium imaging across multiple cortical layers using sculpted light. *Methods* (2016).
30. Li, N., Daie, K., Svoboda, K. & Druckmann, S. Robust neuronal dynamics in premotor cortex during motor planning. Nature 532, 459–464 (2016)
31. Dombeck, D. A., Harvey, C. D., Tian, L., Looger, L. L. & Tank, D. W. Functional imaging of hippocampal place cells at cellular resolution during virtual navigation. Nat. Neurosci. 13, 1433–1440 (2010)
32. Marshel, J. H., Kaye, A. P., Nauhaus, I. & Callaway, E. M. Anterior-posterior direction opponency in the superficial mouse lateral geniculate nucleus. Neuron 76, 713–720 (2012)
33. Stamatakis, A. M. et al. Simultaneous Optogenetics and Cellular Resolution Calcium Imaging During Active Behavior Using a Miniaturized Microscope. Front. Neurosci. 12, 496 (2018)
34. Pluta, S. *et al.* A direct translaminar inhibitory circuit tunes cortical output. *Neurosci.* **18**, 1631–1640 (2015).

Figures

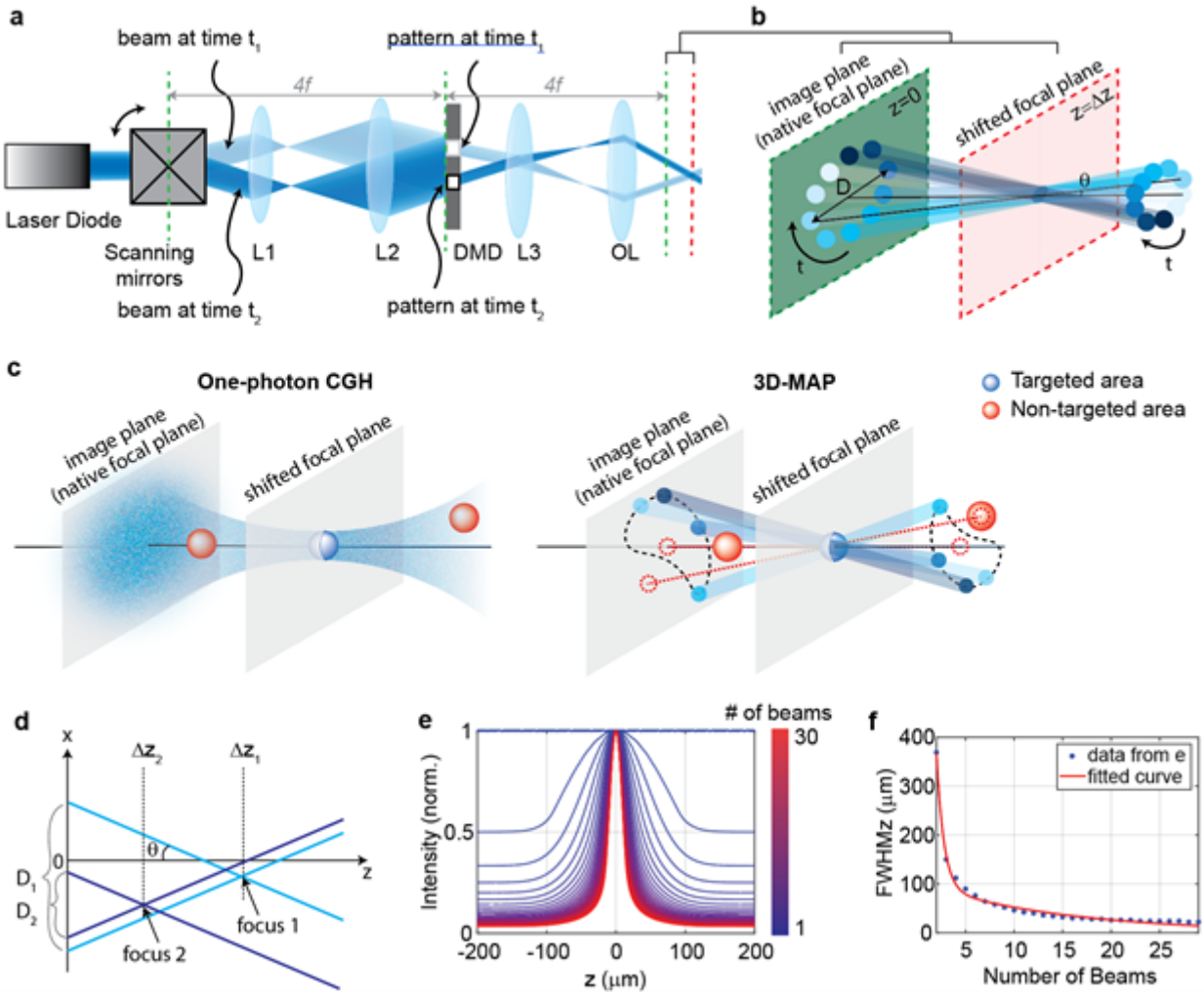

Figure 1

Experimental setup for Three-dimensional random Access Photostimulation (3D-MAP). (a) A collimated laser beam illuminates the surface of a DMD with a custom illumination angle set by scanning mirrors. The DMD is synchronized with the scanning mirrors to project the corresponding 2D amplitude mask of spatial aperture along the given illumination angle. (b) Detailed view of the overlapping amplitude masks and illumination angles at the conjugate image plane (green) and how synchronized illumination angles and amplitude masks can generate a focus at the shifted focal plane (red). Circular patterns labeled by different colors are spatial apertures projected at different times. The position illuminated by all beams while sweeping through each illumination angle forms a focus at the shifted focal plane at z=Δz. D is the diameter of the sweeping trace. θ is the illumination angle. (c) A focus generated by CGH stimulates the targeted area (blue) in focus but also stimulates non-targeted areas (red) out of focus. 3D-MAP is able to stimulate only the targeted areas and avoid non-targeted areas by close the amplitude apertures in that perspective angles (dashed red line). (d) Multiple foci can be generated simultaneously at various depths by superposition of their perspective projection along each illumination angle. (e) Simulated maximum intensity profile along the z-axis for an increasing number of overlapping beams shows the improvement of axial resolution. (f) Full width at half maximums (FWHMs) of the illumination patterns in (e). The case of one beam is excluded because it has no z-sectioning ability.

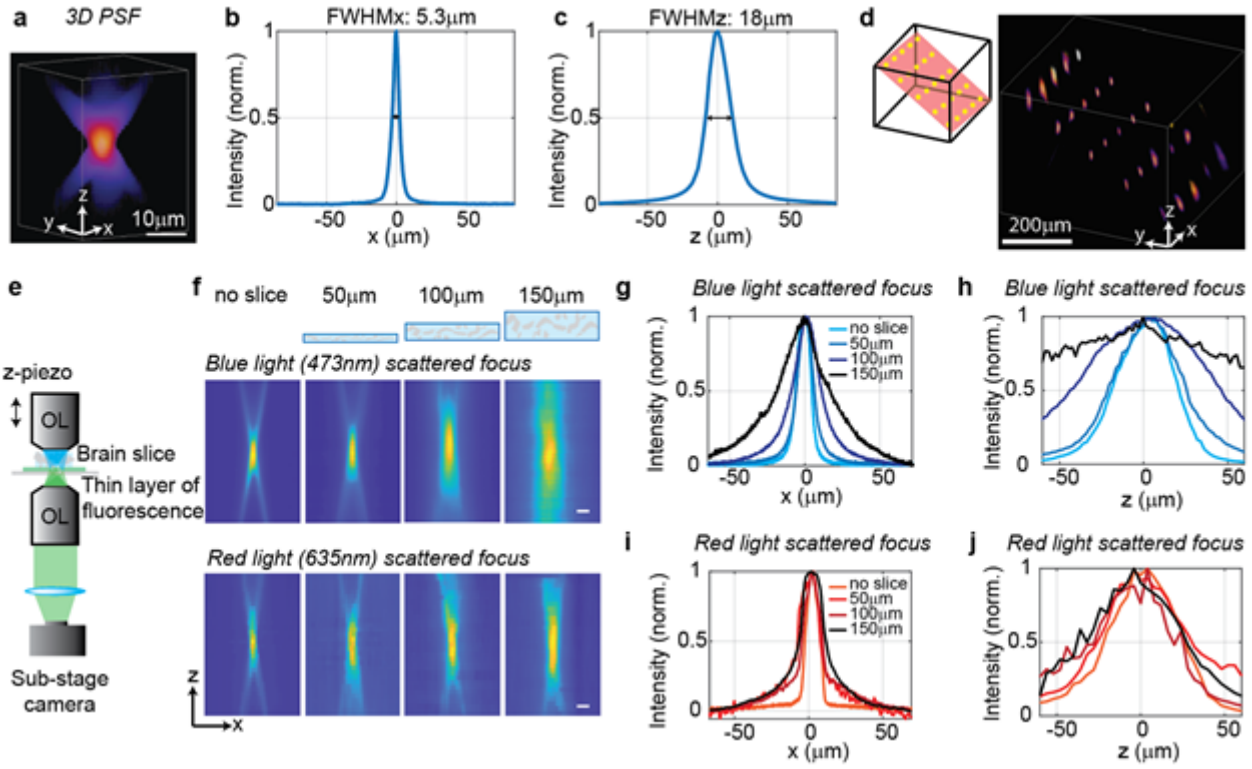

Figure 2

Optical characterization of the spatial resolution of 3D-MAP with and without scattering. (a) Experimentally measured 3D optical PSF (1-pixel aperture on DMD) built up from images of a thin, uniform fluorescent calibration slide recorded at different depths using a sub-stage camera. (b) The PSF's lateral cross-section (x-axis) has a FWHM of 5.3μm. (c) The PSF axial cross-section (z-axis) has a FWHM of 18μm. (d) Left: we simultaneously generated 25 foci spanning across a large volume. Right, experimental measurement of the corresponding 3D fluorescence distribution. (e) Schematic diagram of the sub-stage microscope assembly for 3D pattern measurement. To characterize the effects of tissue scattering we experimentally measured foci generated by a 10-pixel radius aperture on DMD through brain slices of different thickness (0-150μm) using the sub-stage microscope. Notice that (a-c) is the spatial resolution of the system and (e-j) is on purposely enlarged the target size to match the size of neurons. (f) XZ cross-section of the scattered PSF, measured with blue and red light stimulation respectively. Scale bar, 10μm. (g) Under blue light illumination, the FWHM along the x-axis for increased amounts of scattering is 11.7μm, 12.2μm, 19.7μm, and 29.0μm. (h) With blue light illumination, the FWHM along the z-axis is 42μm, 46μm, 76μm and 122μm. (i) With red light illumination, the FWHM along the x-axis for increased amounts of scattering is 10.4μm, 19.3μm, 26.7μm, and 29.6μm. (j) Under red light illumination, the FWHM along the z-axis for increased amounts of scattering is 50.7μm, 75.4μm, 79.7μm, and 73.1μm.

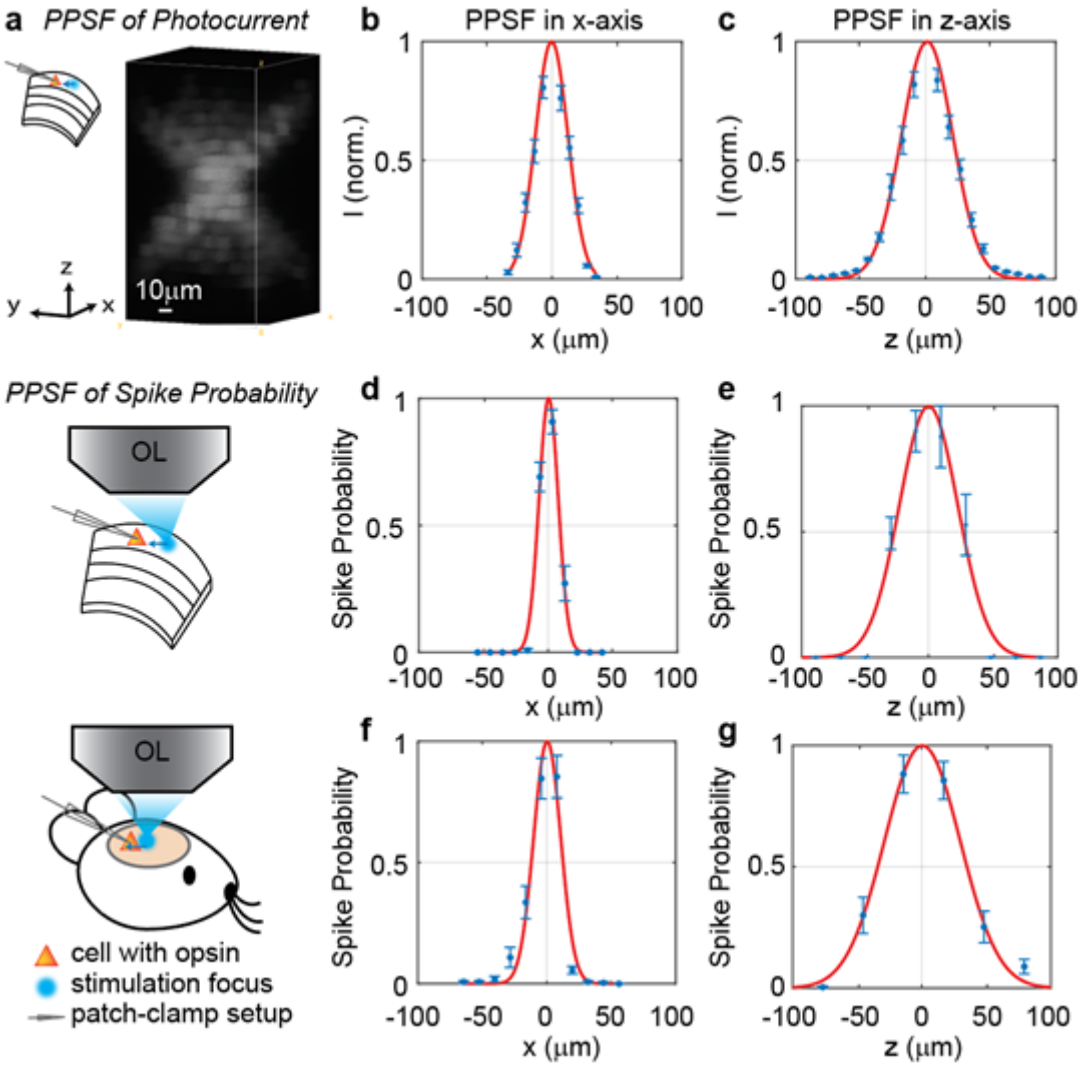

Figure 3

3D-MAP provides high spatial resolution photo-activation of neurons in vitro and in vivo. PPSF, physiological point spread function. (a) Example image of a 3D PPSF measurement in vitro. (b-c) Photocurrent resolution (FWHM) is 29±0.8μm laterally, and 44±1.6μm axially (n=9 neurons). (d-e) 3D-MAP evoked spiking resolution in brain slices is 16±2.4μm laterally and 44±8.9μm axially (n=5 neurons). (f-g) 3D-MAP evoked spiking resolution measured in vivo is 19±3.7μm laterally and 45±6.1μm axially (n=8 neurons). The data represents the mean ± s.e.m (standard error of the mean) for all plots.

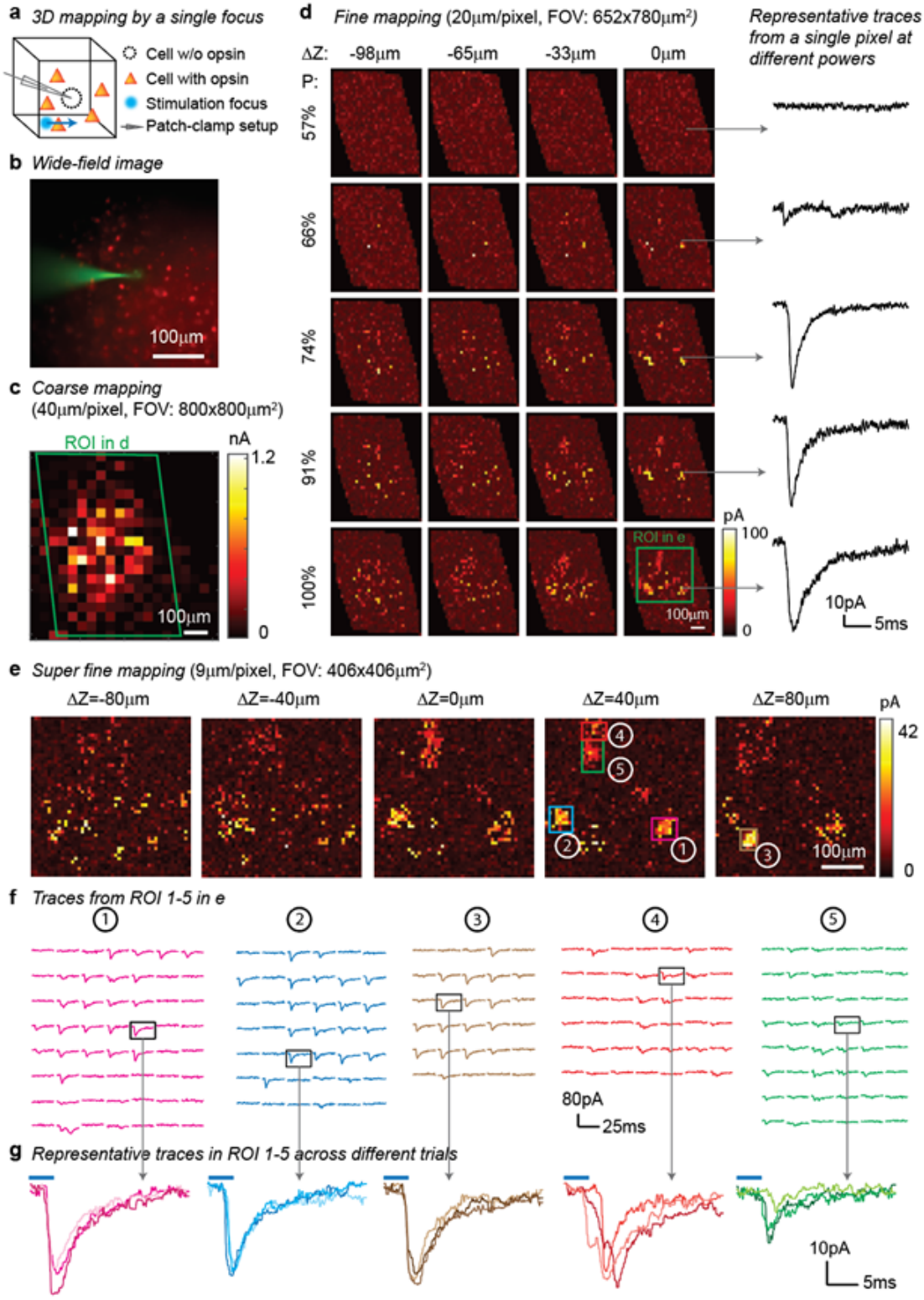

Figure 4

3D Mapping of excitatory synaptic connections with 3D-MAP. (a) Schematic diagram of the experiment. A single focus randomly scans the volume adjacent to the patched interneuron (which does not express opsin), and the readout map reveals the synaptic connections between photo-activated pyramidal neurons and the patched interneuron. (b) Example of widefield image of opsin-expressing pyramidal neurons (red) and the patched interneuron (green). (c) A coarse 2D map in an 800x800μm2 FOV at 40μm

resolution identifies the sub-region of the brain slice with presynaptic neurons. (d) Mapping the selected region at higher resolution (green box in c). Each row uses the same stimulation laser power (100% power: 145μW) across multiple axial planes, and each column is a map of the same axial plane at different powers. Representative excitatory postsynaptic currents (EPSCs) traces on the right show how synaptic currents at the same photostimulation pixel change as the stimulation power increases, presumably due to recruitment of additional presynaptic neurons. Data are averaged over 5 repetitions. (e) Super-fine resolution mapping of the region of interest (ROI) (green box in d) in 3D at P=90μW. (f) Traces from ROIs 1-5 labeled in e, averaged over 5 repetitions. (g) Representative traces of single trials without averaging from corresponding ROIs in the same color, measured across three different repetitions. The blue bar on top of traces indicates the 4ms stimulation time.

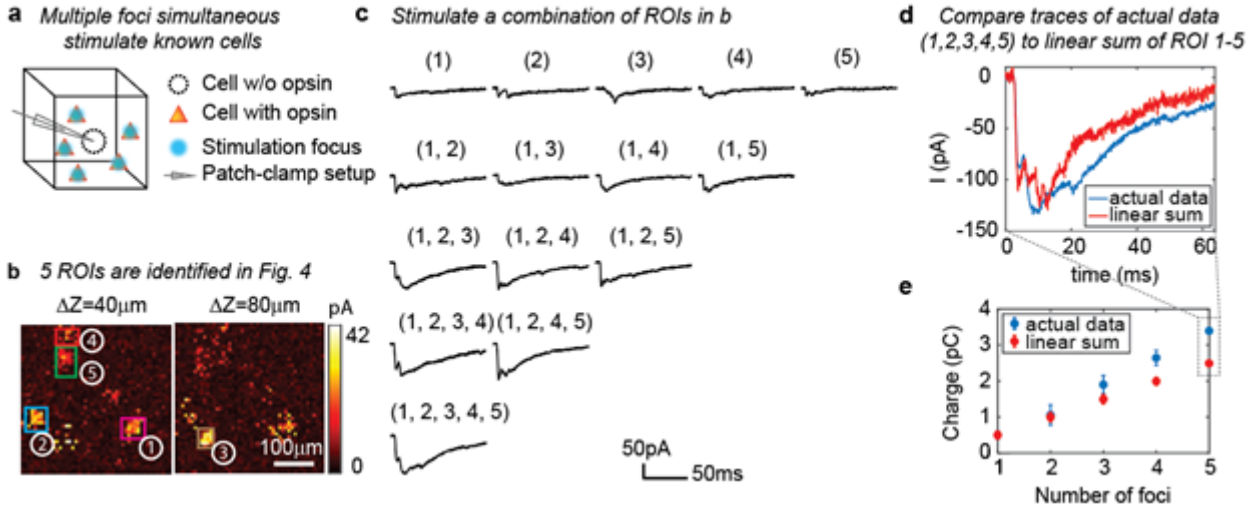

Figure 5

3D-MAP is able to stimulate multiple targets simultaneously to explore network dynamics. (a) Schematic diagram of the experiment. The stimulation ROIs are known to have synaptic connections with the patched interneuron from the widefield mapping as described in Fig. 4. (b) The position of 5 ROIs are identified in Fig. 4e. (c) Representative photocurrent traces for simultaneous stimulation of subsets of the 5 ROIs. Traces are averaged over 4 repetitions. The number(s) above each trace indicate the ROIs that were stimulated to generate the response. (d) Comparison of the actual synaptic response by simultaneous stimulation of ROI 1-5 (blue) to the response calculated by linearly summing the traces when stimulating ROI 1-5 individually (red). The individual response from each ROI is shown in the first row of c. (e) Comparison of the integral of the synaptic currents from simultaneous stimulation of multiple connected presynaptic neurons (blue) to the linear sum of the individual stimulation responses (red). The mean and standard deviation of data is calculated from all the k-combinations (number of foci) from the given set of 5 targets. The sample size is C(5,k),k=1,2,3,4,5.

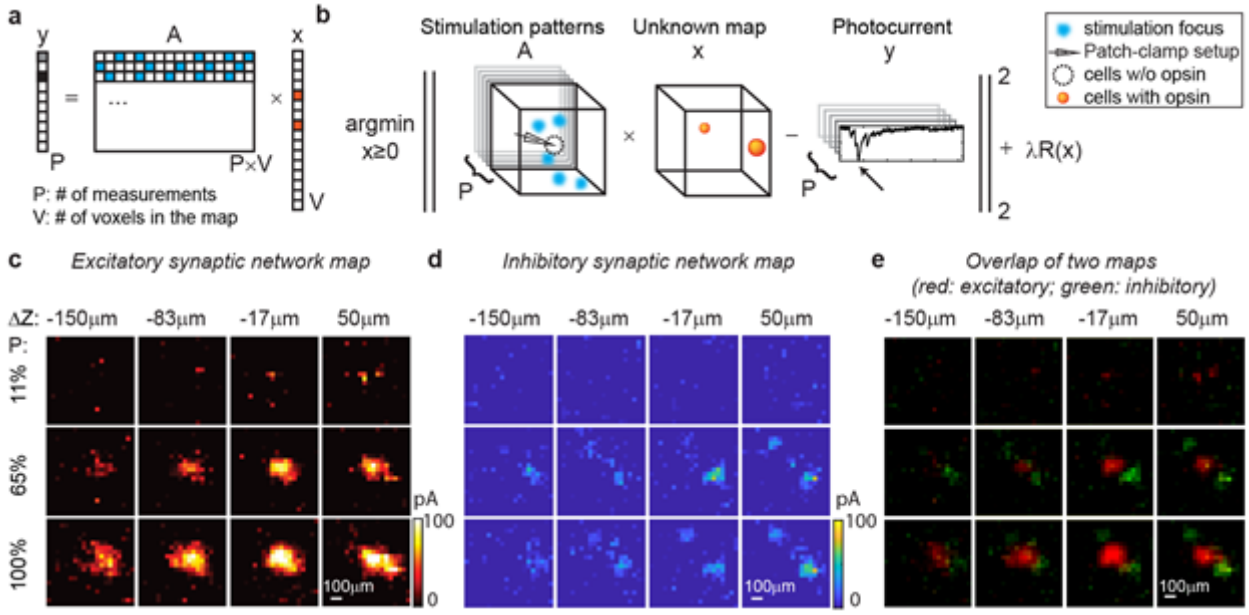

Figure 6

Mapping of synaptic networks in vitro by multi-site random simultaneous stimulation and computational reconstruction. (a) Forward model for multi-site random simultaneous stimulation. V, the number of voxels in the 3D volume. P, the number of patterns, which are orthogonal to each other. y, peak value of the measured synaptic currents. A is a matrix, where each row represents an illumination pattern, including 5 foci here (blue, N=5). x is a vector of the unknown synaptic networks to be reconstructed. (b) Inverse problem formulation. The aim is to approximate x by minimizing the difference between the peak of measured currents (y) and those expected via the forward model with a regularizer λR(x). The details of computational reconstruction framework are in Methods. (c) Excitatory synaptic connection map of a GABAergic interneuron located at [0, 0, 0]. (d) Inhibitory synaptic connection map from the same cell. (e) Overlap of the excitatory map (red) and inhibitory map (green) to show their spatial relationship. Figures in (c-e) are recorded in an 800x800x200μm3 volume at three different stimulation powers (100% stimulation power is 890μW). The number of simultaneous stimulation foci (N) is five in both cases and the results are average over five repetitions.

Supplementary Files

This is a list of supplementary files associated with this preprint. Click to download.

- ReportingSummary.pdf
- FigS1.png
- FigS2.png
- FigS3.png
- FigS4.png
- TableS1.png